Supplementary for

Measurement report: Quantifying source contribution and radiative forcing of fossil fuel and biomass burning black carbon aerosol in the southeastern margin of Tibetan Plateau

Huikun Liu[1,2,3], Qiyuan Wang[1,2,3,4*], Li Xing[5], Yong Zhang[2,3], Ting Zhang,[1,2], Weikang Ran[2], Junji Cao[1,2,3,4*]

[1]State Key Laboratory of Loess and Quaternary Geology, Institute of Earth Environment, Chinese Academy of Sciences, Xi'an, 710061, China
[2]Key Laboratory of Aerosol Chemistry and Physics, Institute of Earth Environment, Chinese Academy of Sciences, Xi'an, 710061, China
[3]University of Chinese Academy of Sciences, Beijing, 100049, China
[4]CAS Center for Excellence in Quaternary Science and Global Change, Xi'an, 710061, China
[5]School of Geography and Tourism, Shaanxi Normal University, Xi'an, 710119, China

Correspondence to: Qiyuan Wang (wangqy@ieecas.cn) and Junji Cao (cao@loess.llqg.ac.cn)

Text S1. Chemical composition measurements

S1.1 Wate-soluble ions analysis

The concentrations of K^+ was determined by a Dionex DX-600 ion chromatograph (IC, Dionex Inc., Sunnyvale, CA, USA). The instrument was equipped with IonPac CS12A column (20m Methane sulfonic acid as the eluent) for cation analysis. QA/QC were conducted based on the Standard reference materials produced by the National Research Center for Certified Reference Materials in China. To extract the water-soluble ions from the quartz filters, a quarter of each weighed filter was placed in a separate 15 mL vials containing 10 mL distilled deionized water (18.2 MΩ resistivity). The vials were placed in an ultrasonic water bath and shaken with a mechanical shaker for 1 h to extract the ions. The extracts were filtered through 0.45 μm pore size microporous membranes, and the filtrates were stored at 4 °C in clean tubes before instrumental analysis.

S1.2 OC/EC analysis

Elemental carbon (EC) and organic carbon (OC) were analysed by a DRI Model 2001 Thermal/Optical Carbon Analyzer (Atmoslytic Inc., Calabasas, CA, USA) with the thermal/optical reflectance (TOR) method. The IMPROVE_A protocol was used for the analysis. A punch aliquot of a quartz filter sample was heated in a stepwise manner to obtain data for four OC fractions (OC1, OC2, OC3, and OC4) in a helium atmosphere at 140°C，280°C，480°C，580°C, and three EC fractions (EC1, EC2, and EC3) in a 2% oxygen, 98% helium atmosphere at 580°C, 740°C, 840°C. At the same time, pyrolyzed carbon (OP) was produced at <580°C in the inert atmosphere, this component decreases the reflected light to correct for charred OC. Total OC is defined as the sum of the four OC fractions plus OP, and total EC is the sum of the three EC fractions minus OP. Specific quality assurance/quality control (QA/QC) procedures for these analyses have been described in detail in Cao et al., (2003).

S1.3 Elemental analysis

Elements including S, Ca, Ti, Mn, Fe, Cu, As, Br, Pb and Zn were quantified by energy-dispersive X-ray fluorescence (ED-XRF) spectrometry (Epsilon 5 ED-XRF, PANalytical B.V., Netherlands). ED-XRF spectrometry uses a three-dimensional polarizing geometry with eleven secondary targets and one barkla target. Good signal to background ratio and low detection limits were achieved. The X-ray source is a side window X-ray tube with a gadolinium anode, operated at an accelerating voltage of 25e100 kV and a current of 0.5e24 mA (maximum power: 600 W). The characteristic X-ray radiation is detected by a germanium detector (PAN 32). Each sample was analysed for about 30 minutes to obtain a spectrum of X-ray counts versus photon energy, with the individual peak energies matching specific elements, and peak areas corresponding to elemental concentrations. The ED-XRF spectrometer was calibrated with thin-film standards obtained from MicroMatter Co. (Arlington, WA, USA).

S1.4 Levoglucosan analysis

Filter sample was extracted in 10 mL of distilled deionized water, and 0.45-mm pore size microporous membranes were used to filter out the insoluble material. The extracts were placed in an ultrasonic water bath and shaken with a mechanical shaker. A high-performance anion exchange chromatography with pulsed amperometric detector (HPAEC-PAD) on a Dionex DX-600 ion chromatograph (Dionex Inc., Sunnyvale, CA, USA) was used to quantify the levoglucosan. Levoglucosan was separated by a Dionex CarboPac MA1 analytical column (4 x 250 mm) and a Dionex CarboPac MA1 guard column with sodium hydroxide solution (612 mM) as eluent at the flow rate of 0.4 mL min^{-1}. Aliquots of 100 mL of each extract were introduced into the system. The measurement was 1hr for each sample. The MDL (S/N=3:1) of levoglucosan is 1.3 ng mL^{-1}.

S1.5 Benzothiazolone analysis

Filter samples were extracted in a methanol solvent, the volume was adjusted into 5ml by ratory evaporator with the target analytes in it. Aliquots of 50μL of extracts were

adjusted to PH9.1 by 50μL borate buffer. Later the ultrasound-assisted extraction was applied for the filter samples for 20 minutes. The final solutions were then diluted with 3:1 mixture of water and acetone. The mixture also included 40μL dansyl chloride and 10μL internal standard solution. After 1min agitation in a vortex, the reaction mixture is ready to ultrasound irradiation for 15 minutes at 35°C and the reaction vials were stored in a dark condition. The derivatized products firstly were injected into the HPLC (Series 1200; Agilent Technology) furnished with a Waters Sunfire C18 column (2.1 × 150 mm, 3.5-μm particle size) and coupled with an ion-trap mass spectrometer (Esquire 3000; Bruker Daltonics, Billerica, MA, USA). The minimum detection limit of Benzothiazolone is 0.0153 ng cm^{-2}. The replication analysis of standards demonstrates the precisions were lower than 6.9%.

Table S1 OPAC modelled b_{scat} (M m^{-1}), b_{abs} (M m^{-1}), SSA and PAX measured b_{scat} (M m^{-1}), b_{abs} (M m^{-1}), SSA

Date	PAX b_{abs}(532)	OPAC b_{abs}(550)	b_{abs} difference	PAX b_{scat}(532)	OPAC b_{scat}(550)	b_{scat} difference	SSA PAX	SSA OPAC	SSA difference
2018/3/15	7.47	7.23	-3.24%	61.33	60.20	-1.85%	0.89	0.89	0.07%
2018/3/16	5.82	5.81	-0.25%	62.71	61.40	-2.08%	0.92	0.91	-0.11%
2018/3/17	3.48	3.62	3.96%	84.30	84.30	0.00%	0.96	0.96	-0.14%
2018/3/18	3.75	3.78	0.70%	46.12	44.40	-3.73%	0.92	0.92	-0.30%
2018/3/19	2.60	2.70	3.69%	19.84	20.20	1.82%	0.88	0.88	-0.34%
2018/3/20	3.01	3.02	0.25%	24.98	25.30	1.29%	0.89	0.89	0.18%
2018/3/21	2.62	2.69	2.58%	29.93	30.10	0.58%	0.92	0.92	-0.16%
2018/3/22	8.63	8.53	-1.20%	88.01	89.60	1.81%	0.91	0.91	0.26%
2018/3/23	10.30	10.04	-2.51%	94.02	96.10	2.21%	0.90	0.91	0.41%
2018/3/24	7.85	7.80	-0.69%	76.08	78.30	2.91%	0.91	0.91	0.06%
2018/3/25	7.54	7.74	2.66%	67.48	69.20	2.55%	0.90	0.90	0.06%
2018/3/27	9.46	9.48	0.26%	85.27	86.70	1.68%	0.91	0.90	-0.91%
2018/3/28	2.49	2.50	0.44%	39.34	39.42	0.20%	0.94	0.94	-0.27%
2018/3/29	4.14	4.04	-2.33%	53.20	54.49	2.42%	0.93	0.93	0.34%

2018/3/30	5.92	5.95	0.58%	76.74	77.07	0.43%	0.93	0.93	-0.01%
2018/3/31	4.06	3.98	-1.97%	40.34	39.36	-2.44%	0.91	0.91	-0.06%
2018/4/1	3.32	3.26	-1.72%	35.03	35.14	0.31%	0.91	0.92	0.16%
2018/4/3	3.51	3.50	-0.42%	35.66	35.82	0.44%	0.91	0.91	0.03%
2018/4/4	6.62	6.58	-0.70%	54.47	54.70	0.43%	0.89	0.89	0.05%
2018/4/5	6.55	6.61	0.87%	56.55	55.90	-1.15%	0.90	0.89	-0.20%
2018/4/6	3.07	3.08	0.18%	37.79	37.46	-0.88%	0.92	0.92	-0.09%
2018/4/7	1.51	1.50	-0.34%	14.59	14.70	0.72%	0.91	0.91	0.08%
2018/4/8	4.36	4.42	1.39%	72.50	71.22	-1.77%	0.94	0.94	-0.14%
2018/4/9	2.74	2.78	1.29%	31.25	31.20	-0.18%	0.92	0.92	-0.14%
2018/4/10	2.29	2.27	-0.70%	25.70	25.65	-0.20%	0.92	0.92	-0.04%
2018/4/11	1.88	1.85	-1.48%	23.86	23.45	-1.71%	0.93	0.93	-0.01%
2018/4/12	3.24	3.16	-2.36%	32.51	32.85	1.04%	0.91	0.91	-0.07%
2018/4/13	17.51	17.20	-1.76%	41.31	41.80	1.19%	0.70	0.71	0.81%
2018/4/14	4.37	4.40	0.61%	20.81	20.22	-2.83%	0.83	0.82	-0.61%
2018/4/15	0.75	0.76	1.76%	15.77	15.77	0.02%	0.95	0.95	-0.08%
2018/4/16	2.20	2.21	0.52%	28.55	28.73	0.64%	0.93	0.93	-0.05%

2018/4/17	4.75	4.77	0.54%	43.22	43.09	-0.30%	0.90	0.90	-0.12%
2018/4/18	6.76	6.80	0.54%	81.87	81.27	-0.73%	0.92	0.92	-0.10%
2018/4/19	3.06	3.05	-0.34%	66.41	66.53	0.18%	0.96	0.96	0.01%
2018/4/20	2.36	2.4	1.62%	25.87	25.87	-0.02%	0.92	0.91	-0.45%
2018/4/21	3.34	3.35	0.27%	46.69	46.72	0.07%	0.93	0.93	-0.03%
2018/4/22	3.14	3.09	-1.57%	45.00	45.75	1.66%	0.93	0.94	0.13%
2018/4/23	2.61	2.68	2.76%	25.13	25.54	1.62%	0.91	0.91	0.25%
2018/4/24	3.93	3.88	-1.38%	36.72	36.68	-0.10%	0.90	0.90	0.12%
2018/4/25	5.52	5.54	0.43%	48.44	48.59	0.31%	0.90	0.90	-0.03%
2018/4/26	10.49	10.42	-0.70%	89.62	90.06	0.49%	0.90	0.89	-0.18%
2018/4/27	7.44	7.20	-3.35%	73.20	73.77	0.78%	0.91	0.91	0.37%
2018/4/28	7.74	7.66	-1.05%	77.17	77.59	0.54%	0.91	0.91	0.17%
2018/4/29	5.76	5.85	1.50%	57.98	57.47	-0.87%	0.91	0.91	-0.22%
2018/4/30	3.93	4.03	2.53%	85.00	85.40	0.47%	0.96	0.96	-0.09%
2018/5/1	4.92	4.97	0.99%	62.85	63.23	0.60%	0.93	0.93	-0.02%
2018/5/2	4.42	4.42	-0.08%	71.81	71.42	-0.55%	0.94	0.94	-0.11%
2018/5/3	2.72	2.75	1.23%	54.48	54.01	-0.87%	0.95	0.95	-0.10%

2018/5/4	2.26	2.29	1.18%	47.52	47.46	-0.12%	0.95	0.95	-0.05%
2018/5/5	0.45	0.45	0.86%	15.19	15.14	-0.35%	0.97	0.97	-0.03%
2018/5/6	0.90	0.93	3.01%	22.21	21.60	-2.74%	0.96	0.96	-0.41%
2018/5/7	1.56	1.54	-1.20%	21.75	21.77	0.08%	0.93	0.93	0.09%
2018/5/8	1.27	1.28	0.53%	26.74	26.36	-1.41%	0.95	0.95	-0.09%
2018/5/9	1.77	1.71	-3.33%	23.71	23.90	0.82%	0.93	0.93	0.30%
2018/5/10	1.20	1.22	1.49%	13.55	13.57	0.13%	0.92	0.92	-0.10%
2018/5/11	1.37	1.36	-0.53%	14.47	14.23	-1.66%	0.91	0.91	-0.10%

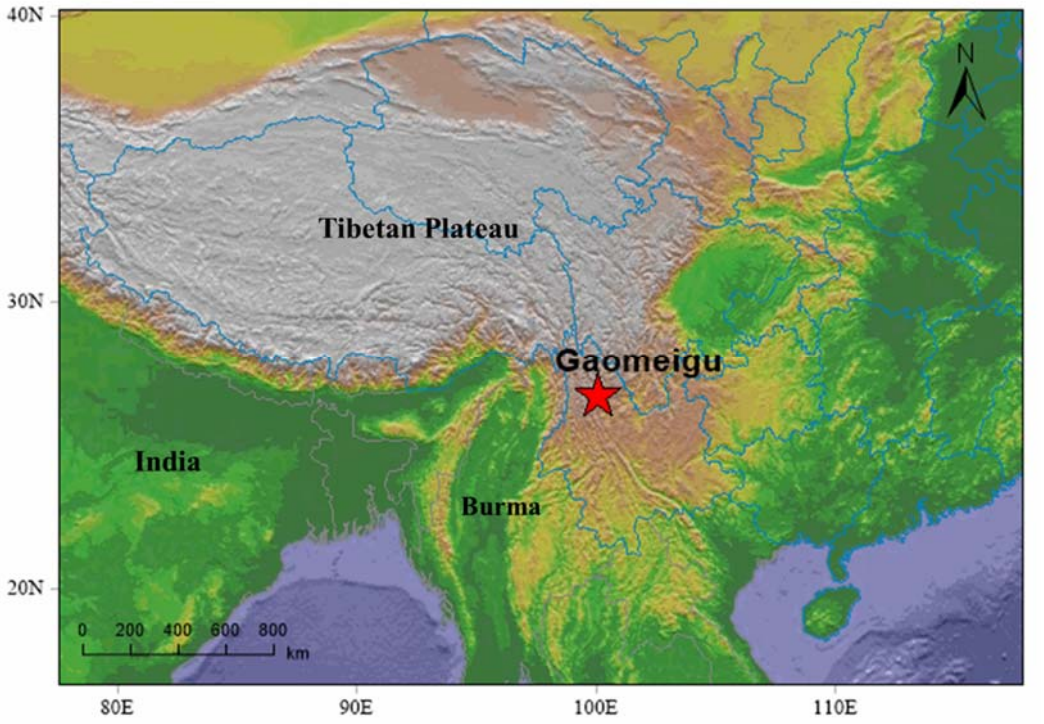

Figure S1. Sampling site in the southeastern margin of Tibetan Plateau and the surrounding region.

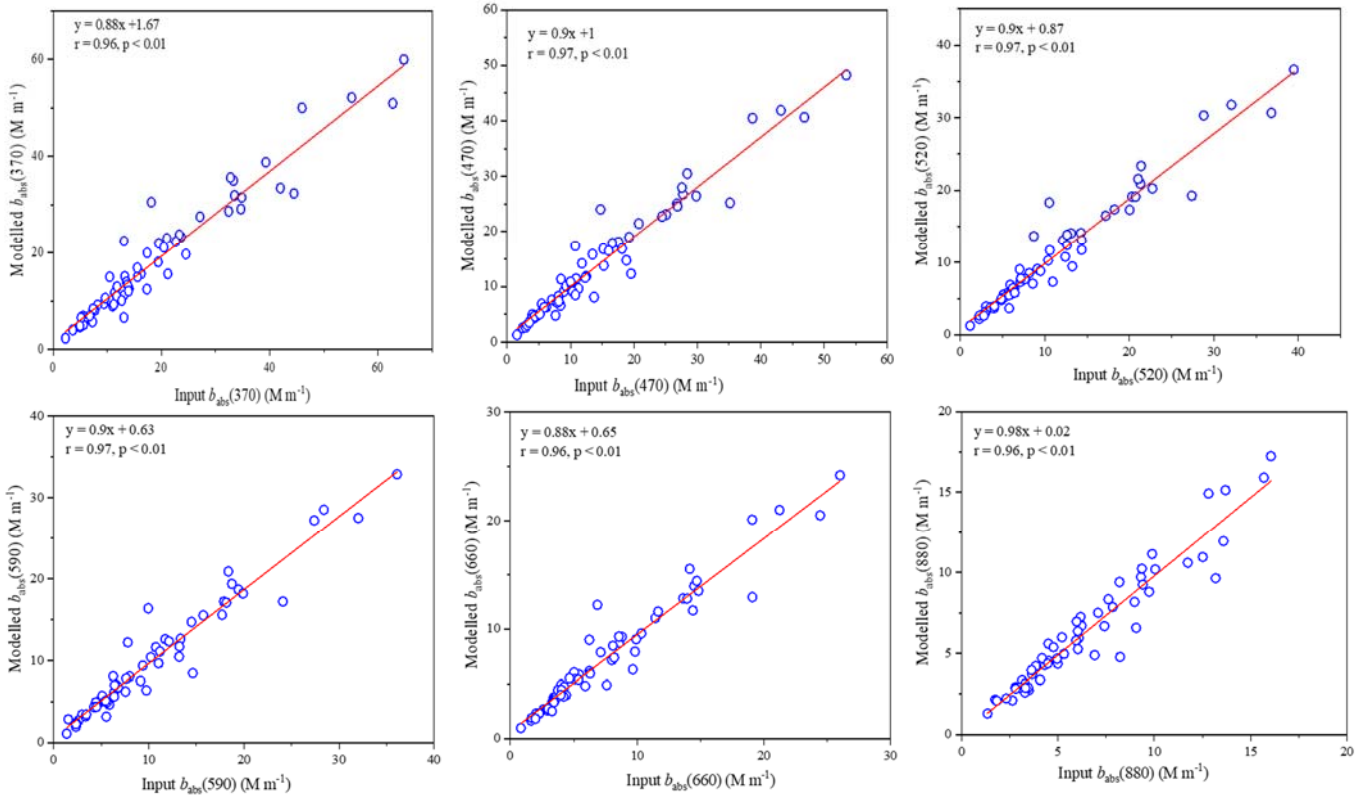

Figure S2. Correlations between the modelled primary $b_{abs}(\lambda)$ by positive matrix factorization and the input ones estimated using black carbon-tracer method. λ represents the wavelengths of 370, 470, 520, 590, 660, or 880 nm.

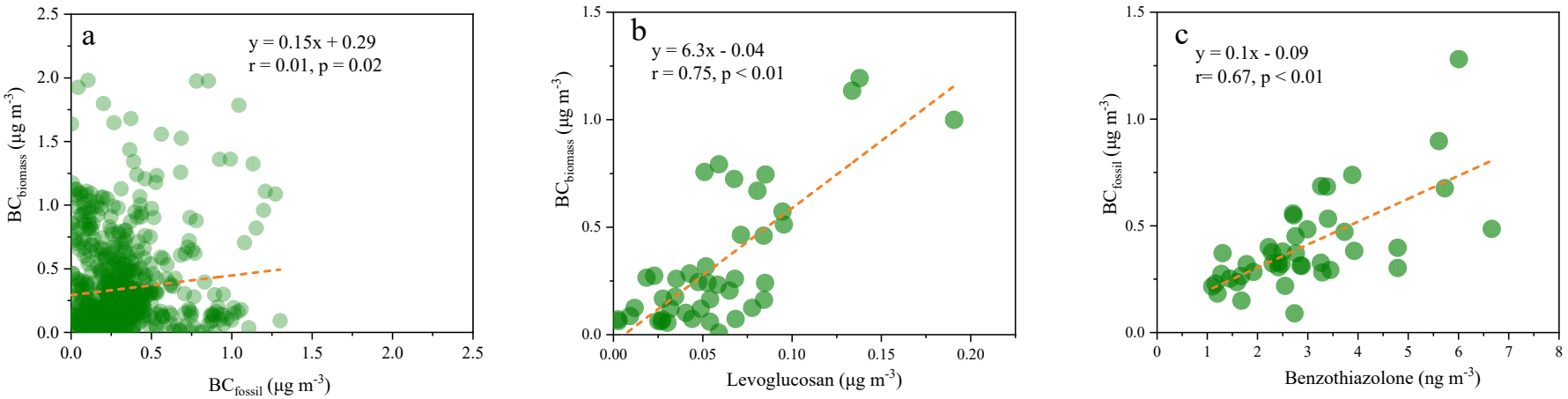

Figure S3. Scatter plots of (a) biomass burning BC ($BC_{biomass}$) versus fossil fuel combustion BC (BC_{fossil}), (b) $BC_{biomass}$ versus levoglucosan, and (c) BC_{fossil} versus benzothiazolone. $BC_{biomass}$ and BC_{fossil} represent black carbon aerosol contributed by biomass burning and fossil fuel sources, respectively.

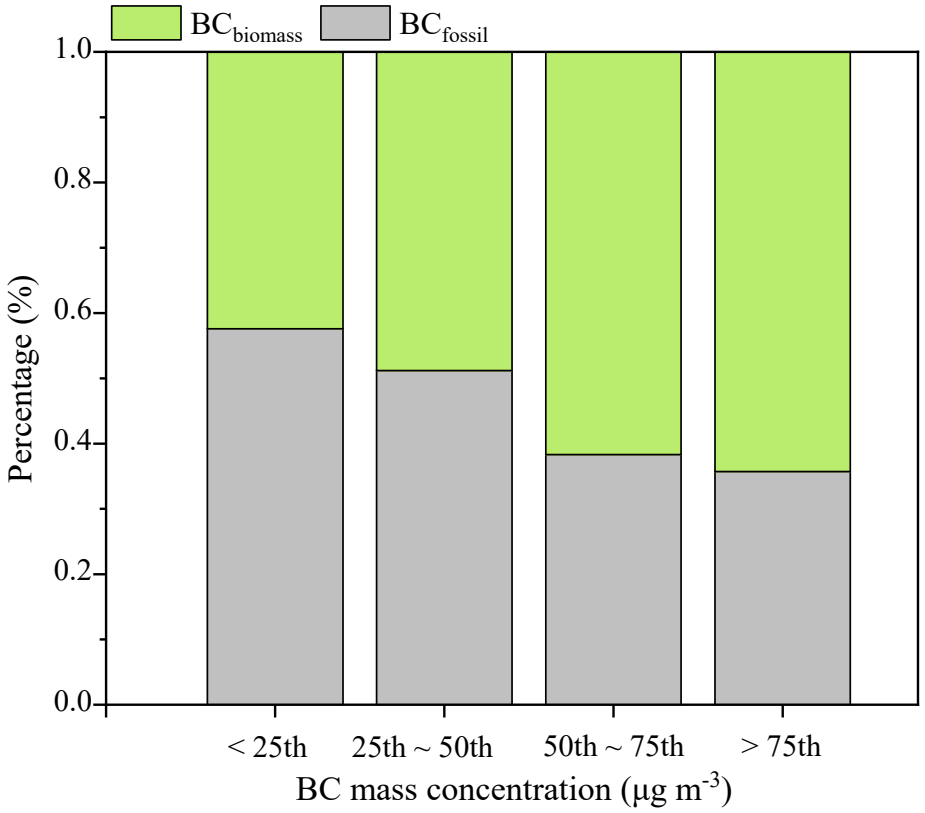

Figure S4. Mass fractions of black carbon (BC) from biomass burning ($BC_{biomass}$) and BC from fossil fuel combustion (BC_{fossil}) in different percentiles of total BC mass concentration.

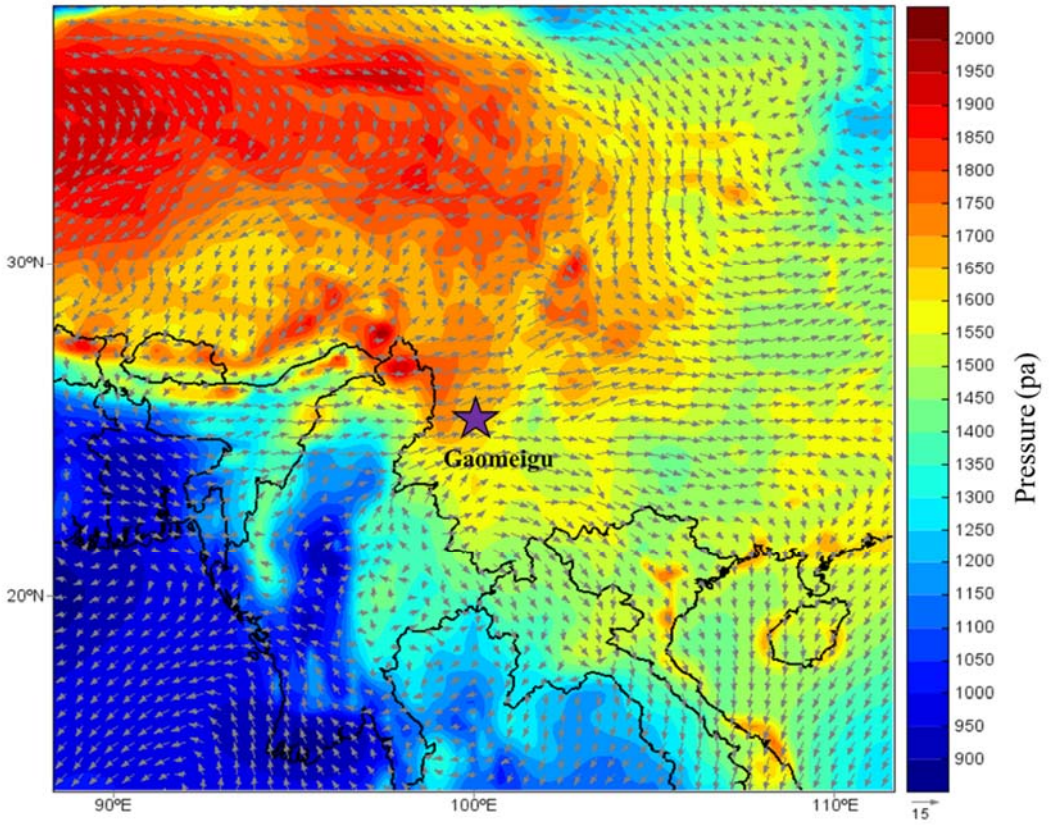

Figure S5. Spatial distribution of morning (8am -12am) wind direction, speed (m s^{-1}) and pressure (Pa). The red start represents the sampling site.

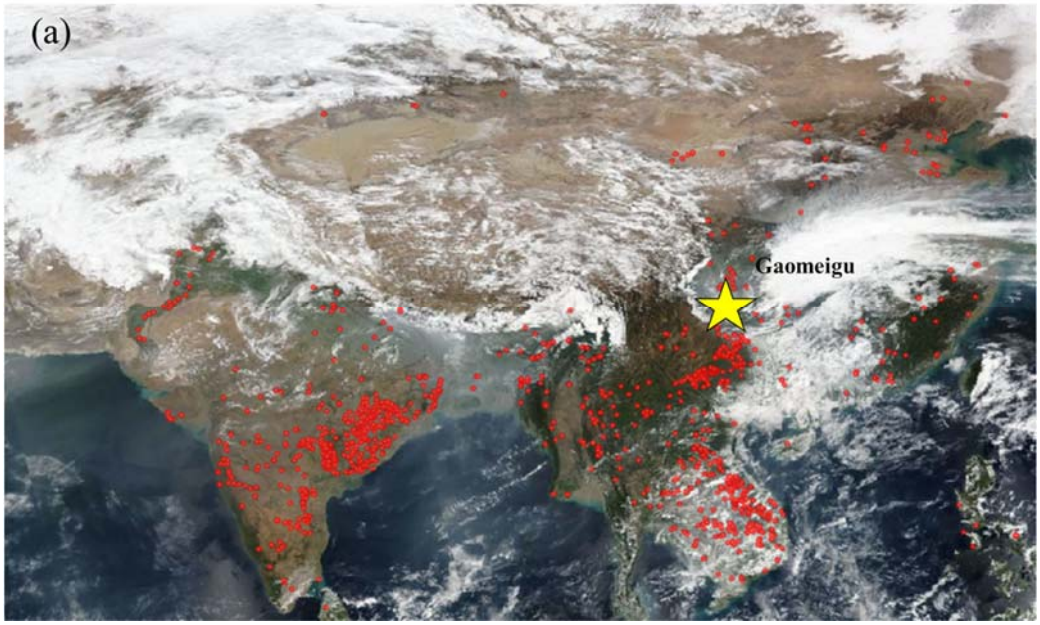
(a)
Gaomeigu

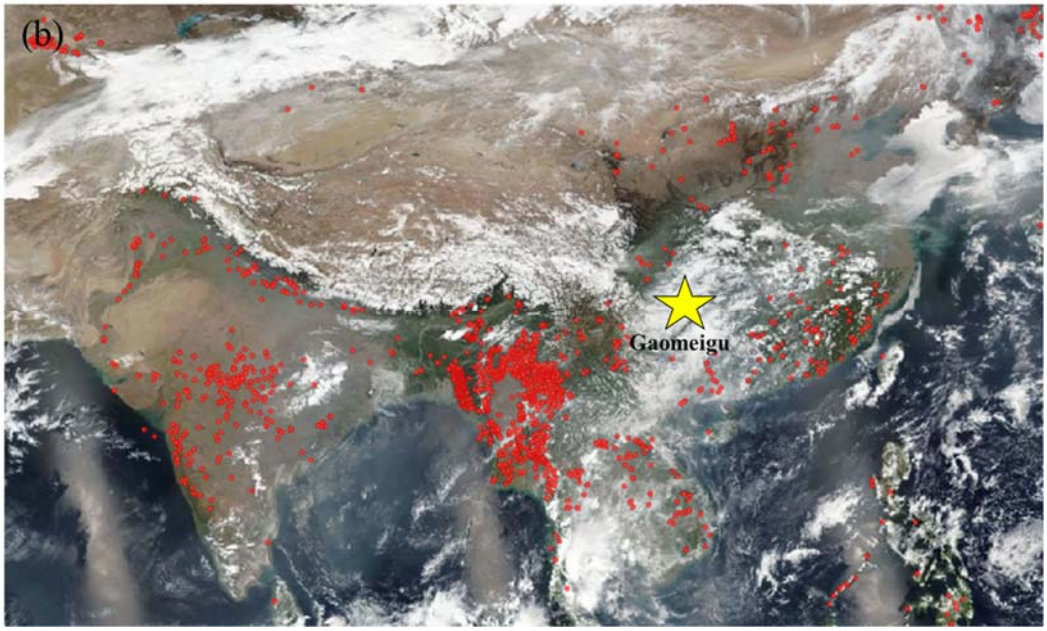
(b)
Gaomeigu

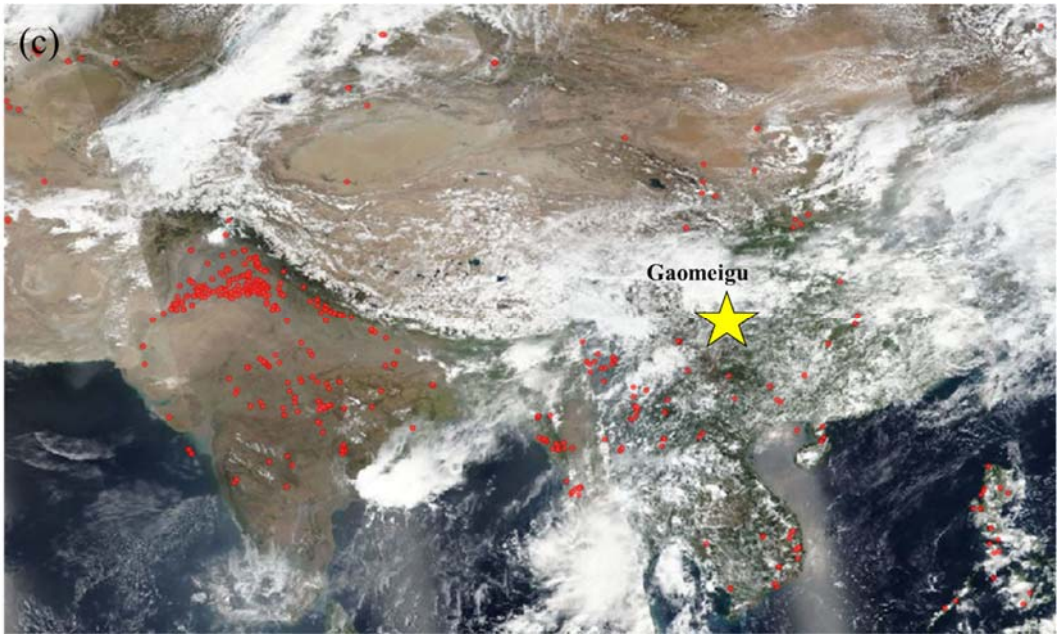

Figure S6. (a) Monthly average fire site map in March in 2018, (b) April in 2018, (c) May in 2018. The fire site map (a), (b), (c) are from © NASA (National Aeronautics and Space Administration) (https://www.nasa.gov/image-feature/goddard/2018/a-world-on-fire)

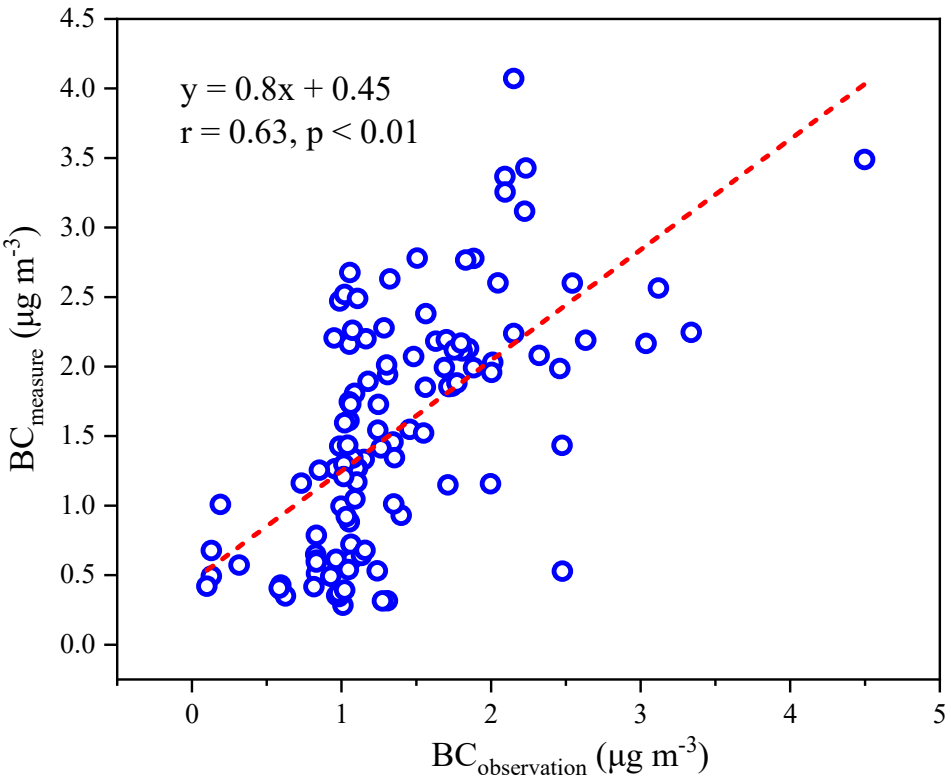

Figure S7. Scatter plots of the black carbon (BC) mass concentration from observation and the ones modelled by WRF-Chem.

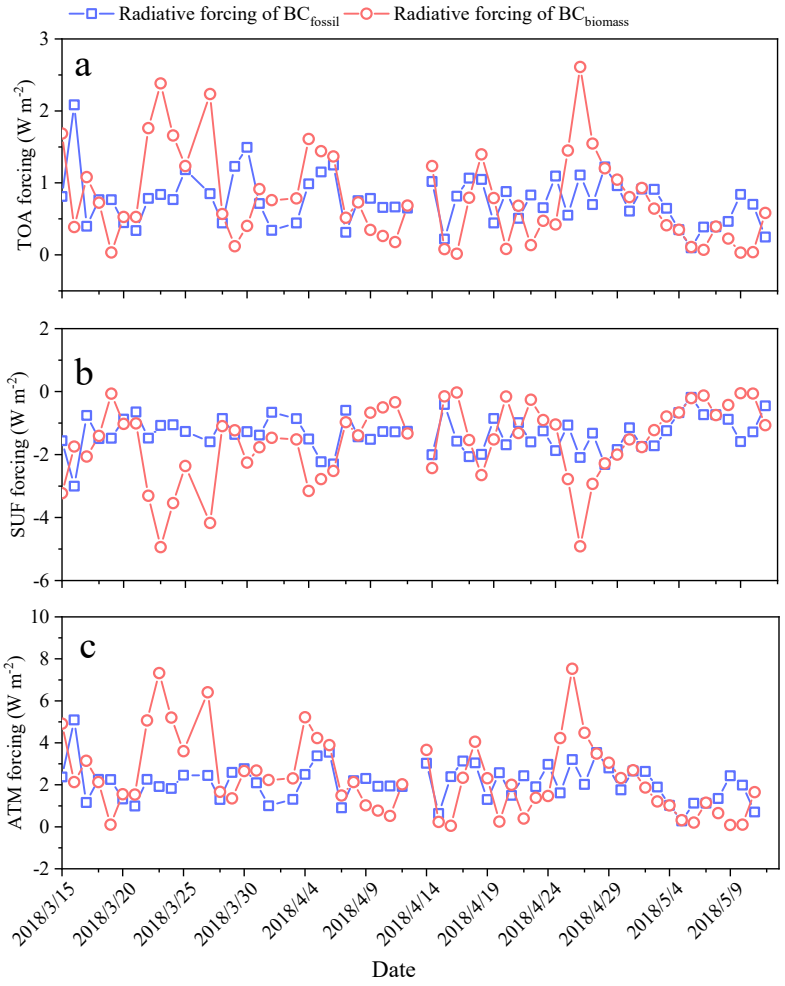

Figure S8. (a) Daily radiative forcing of black carbon (BC) from biomass burning ($BC_{biomass}$) and BC from fossil fuel combustion (BC_{fossil}) at the top of atmsphere (TOA) forcing, (b) at the surface (SUF), and (c) in the atmosphere (ATM).

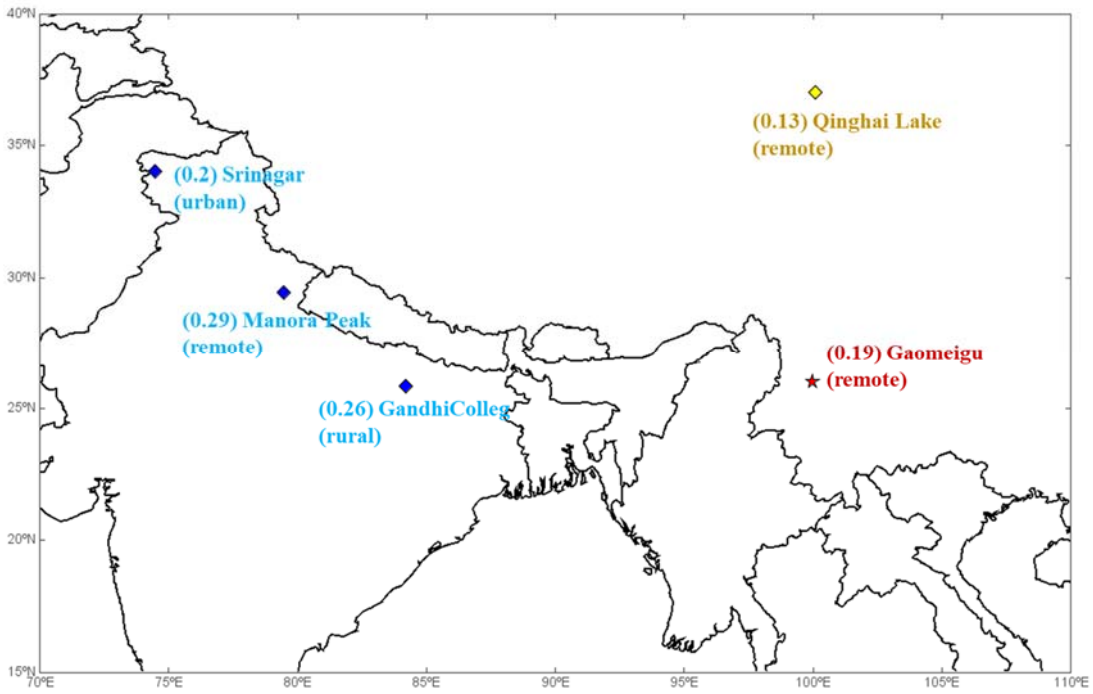

Figure S9. Heating rate per black carbon (BC) concentration ((K day^{-1}) (μg m^{-3})$^{-1}$) at Himalaya and Tibetan Plateau from previous studies (Srivastava et al., 2012; Tiwari et al., 2016; Bhat et al., 2017; Wang et al., 2015).

Reference

Bhat, M. A., Romshoo, S. A., and Beig, G.: Aerosol black carbon at an urban site-Srinagar, Northwestern Himalaya, India: Seasonality, sources, meteorology and radiative forcing, Atmos. Environ., 165, 336-348, 10.1016/j.atmosenv.2017.07.004, 2017.

Cao, J. J., Lee, S. C., Ho, K. F., Zhang, X. Y., Zou, S. C., Fung, K., Chow, J. C., and Watson, J. G.: Characteristics of carbonaceous aerosol in Pearl River Delta Region, China during 2001 winter period, Atmos. Environ., 37, 1451-1460, 10.1016/S1352-2310(02)01002-6, 2003.

Srivastava, A. K., Ram, K., Pant, P., Hegde, P., and Joshi, H.: Black carbon aerosols over Manora Peak in the Indian Himalayan foothills: implications for climate forcing, Environmental Research Letters, 7, 10.1088/1748-9326/7/1/014002, 2012.

Tiwari, S., Dumka, U. C., Hopke, P. K., Tunved, P., Srivastava, A. K., Bisht, D. S., and Chakrabarty, R. K.: Atmospheric heating due to black carbon aerosol during the summer monsoon period over Ballia: A rural environment over Indo-Gangetic Plain, Atmospheric Research, 178-179, 393-400, 10.1016/j.atmosres.2016.04.008, 2016.

Wang, Q. Y., Huang, R. J., Cao, J. J., Tie, X. X., Ni, H. Y., Zhou, Y. Q., Han, Y. M., Hu, T. F., Zhu, C. S., Feng, T., Li, N., and Li, J. D.: Black carbon aerosol in winter northeastern Qinghai–Tibetan Plateau, China: the source, mixing state and optical property, Atmos. Chem. Phys., 15, 13059-13069, 10.5194/acp-15-13059-2015, 2015.